http://www.jourmag.org/index.php/jma

Journal of Magnetism and Its Applications

Received July22nd 2021 received in revised September27th 2021 accepted December 28th 2021

Research article

Impact of $NiCo_2O_4$ Composition on Methylene Blue Photodegradation by $Fe_3O_4/NiCo_2O_4$ Nanocomposites

Sholihatul Mardliyah[1], Sunaryono Sunaryono[1,2]*

[1]Department of Physics, Faculty of Mathematics and Natural Sciences, Universitas Negeri Malang, Jl. Semarang No. 5, Malang 65145, Indonesia
[2]PUI-PT Center of Advanced Materials for Renewable Energy (CAMRY), Universitas Negeri Malang, Jl. Semarang No. 5 Malang 65145, Indonesia

Article info

Keywords:
$Fe_3O_4/NiCo_2O_4$
Nanocomposite
Methylene Blue
Photodegradation
Iron sand

Abstract

$Fe_3O_4/NiCo_2O_4$ nanocomposites were successfully fabricated using the coprecipitation method. The fabrication of $Fe_3O_4/NiCo_2O_4$ nanocomposites were carried out by varying the mass percentage of $NiCo_2O_4$ with a composition of 0%, 15%, 30%, 45%, and 100% of the mass of Fe_3O_4. The characterization of the functional groups of $Fe_3O_4/NiCo_2O_4$ nanocomposites was carried out using the FTIR instrument which showed the functional group bonds of the sample corresponding to the constituent atoms. The characterization of the crystal structure of $Fe_3O_4/NiCo_2O_4$ nanocomposites was carried out using an XRD instrument which showed the appearance of characteristic peaks of the Fe_3O_4 and the $NiCo_2O_4$ phases in the X-ray diffraction patterns. The surface morphology of the $Fe_3O_4/NiCo_2O_4$ nanocomposites was characterized using the SEM instrument which produces an image of the surface morphology of the sample. Potential applications of $Fe_3O_4/NiCo_2O_4$ as photodegradation material for methylene blue (MB) were characterized using a UV-Vis instrument and showed that the $Fe_3O_4/NiCo_2O_4$ nanocomposites can be used for water purification with a degradation percentage of 11.99%. The highest absorbance values of the $Fe_3O_4/NiCo_2O_4$ nanocomposites with UV irradiation for interval of 60, 120, and 180 minutes located at wavelength of 613 and 663 nm.

1. Introduction

Water is the most important substance in the life of all living things. The living things are composed of water and will always live in an environment dominated by water [1]. Thus, it is necessary to control the quantity and quality of water [2]. This is in line with the development of the textile industry, which is growing very rapidly in Indonesia, resulting in some environmental pollution and damage to ecosystems that negatively impact human health and other living things [3]. One of the damages was caused by the processing of liquid waste in the form of synthetic dyes that did not reach the standard while these substances were difficult to degrade [4]. Thus, the waste requires handling or cleaning before being dumped into the river [5]. One of the widely used dyes in this industry is methylene blue (MB) [6]. On the other hand, MB is also included in achromatic compounds that are toxic and carcinogenic. Therefore, waste pollution due to MB left untreated and untreated will have a very negative impact on living things [7]. One of the steps to purify water due to textile dyes is to use materials that can degrade these dyes.

Several researchers carried out studies using the advanced oxidation process method Advanced Oxidation Processes (AOPs) that can be used to degrade dyes into harmless compounds [8]. One method that includes AOPs is photodegradation because it has advantages in efficiency and stability as well as being economical [8]. In principle, the photodegradation method uses a photocatalyst technique, which involves a chemical reaction on exposure to UV light. Where the photocatalyst itself is a process that can accelerate the reduction of metals between Pt [9], Ag [10], Pd [11], the transition metal compounds NiO [12], Co_3O_4 [13], Fe_2O_3 [14, p. 4], NiS [15], CoSx [16], Ni_2P [17], Co_2P [18], FeP [19], and others with the help of light, as well as metal oxides that aim to remove organic dyes [20, 21]. The method of using absorbent material was chosen because it is easy to separate and grade and has high efficiency. Furthermore, it is also economical to use [22]. In addition, to increase the efficiency of the degradation that occurs in the material, other materials that can be used as photocatalysts are also needed, namely magnetite (Fe_3O_4) material. Magnetite Fe_3O_4 material can be used for photocatalyst by having good performance in the photocatalyst process and stability in aqueous media, with magnetic properties that can guarantee efficient separation and catalyst reusability more than once [23]. However, Fe_3O_4 material is difficult to dissolve in water. This creates a new problem by leaving colloid in the purification object [24]. Therefore, it is important to develop other materials that can help the performance of Fe_3O_4 in purifying water but can reduce the formation of residues in the water. One of these materials is nickel cobalt oxide ($NiCo_2O_4$) which is environmentally friendly, and has the potential to be used as a water purification catalyst because it has an active and stable electrocatalyst in alkaline conditions and various wastes.

Previous research showed that the surface area of the $NiCo_2O_4$ material ranges from 16.34; 53.27; 64.17; and 88.85 m^2g^{-1} [25]. In addition, $NiCo_2O_4$ also has a large pore size [26]. So it is suitable for use as an MB photodegradation application. Another study conducted by Chang in 2019 revealed that the $NiCo_2O_4$ material was successfully used as a material to increase the photocatalytic water reduction ability [27]. However, it is still rare to report research that combines the two materials into $Fe_3O_4/NiCo_2O_4$ nanocomposites that have the potential for application of MB dye photodegradation. However, until now, research on the efforts to improve the performance of $NiCo_2O_4$ materials seems sparse [28]. Thus, this study aimed to synthesize and characterize $Fe_3O_4/NiCo_2O_4$ nanocomposites that have the potential to be applied as MB photodegradation materials.

*Corresponding author
Email: sunaryono.fmipa@um.ac.id

DOI: 10.53533/JMA.v1i2.15

2. Experimental Methods

The synthesis of Fe_3O_4 nanoparticles was carried out using the coprecipitation method. The synthesis process began by dissolving 20 g of iron sand into 58 mL of 12M HCl, stirring until a solution of $FeCl_2$ + $FeCl_3$ was formed. The 18 mL solution was combined with 25 mL of NaOH, resulting in a precipitate of Fe_3O_4. In the next phase, the sample was washed to achieve a neutral pH. The process ended with drying the sample using an oven to produce a powder. $NiCo_2O_4$ nanoparticles were carried out using the coprecipitation method, starting with the mixing process of 1.83 g of $Ni(NO_3)_2$ and 3.68 g of $Co(NO_3)_2$ with 150 mL of distilled water as a solvent at room temperature. After that, it was titrated with 50 mL of NaOH so that the solution changed color to dark green, and washed until the pH was neutral. The precipitate obtained was oven-dried for 30 minutes and calcined at temperatures of 200, 220, 250, 275, and 300 ^{0}C to find the sample with the highest crystallinity. Furthermore, Fe_3O_4 and $NiCo_2O_4$ powder (a sample with the highest crystallinity was used based on the results of the crystallinity analysis of the sample from the previous synthesis process) which was produced from the previous synthesis process was composited with variations in mass percent composition (weight presentation) with a total mass of 5 g of nanocomposite. The names of each and the composition of the mass percent $NiCo_2O_4$ samples are as follows: sample FN-0 with 0% of $NiCo_2O_4$, FN-15 with 15% of $NiCo_2O_4$, FN-30 with 30% of $NiCo_2O_4$, FN-45 with 45% of $NiCo_2O_4$, and FN-100 with 100% of $NiCo_2O_4$. The characterizations of the nanocomposites were performed by means of XRD, SEM, FTIR, and UV-Vis spectroscopy.

3. Results and Discussion

The calcined $NiCo_2O_4$ nanoparticles with various temperature were successfully synthesized. The X-ray diffraction pattern of $NiCo_2O_4$ nanoparticles with variations in calcination temperature is presented in Figure 1. The crystallinity values of each variation in calcination temperature was calculated and the results are presented in Table 1. Based on Table 1, the highest crystallinity value was achieved by samples calcined at a temperature of 300 °C, which was 52.62%. This result is almost in agreement with the results of research conducted by Tian et al., which synthesized $NiCo_2O_4$ with a crystallinity of 63.11% [22]. Furthermore, in this study, a calcination temperature of 300 °C was used in the synthesis of $NiCo_2O_4$. Characterization using XRD on each sample variation is shown in Figure 2. Analysis using Rietica software was carried out on each sample by matching the model data with AMCSD 0000945 for the Fe_3O_4 phase and model data with COD number 5000120 and the results are presented in Table 2.

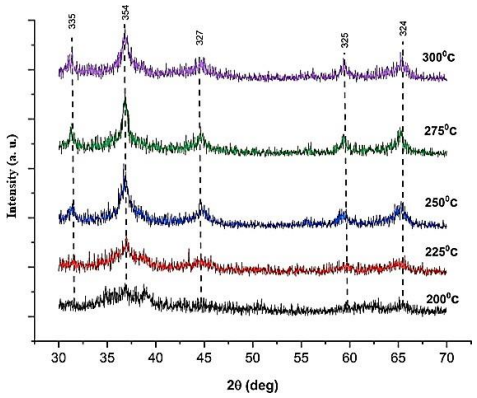


Fig. 1. X-ray diffraction patterns of the $NiCo_2O_4$ nanoparticles with various calcination temperatures

Table 1. Crystallinity of the $NiCo_2O_4$ nanoparticles with various calcination temperatures

Calcination Temperature (°C)	Crystallinity (%)
200	35.62
225	37.04
250	44.62
275	46.44
300	52.62

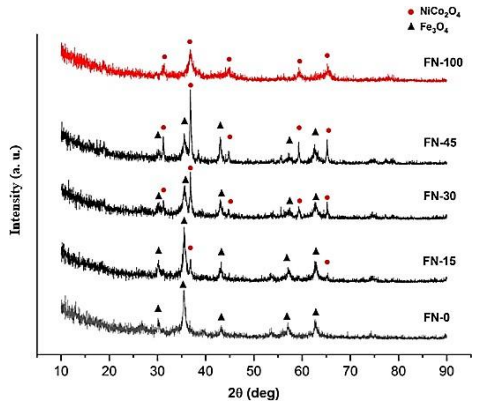


Fig. 2. X-ray diffraction patterns of the $Fe_3O_4/NiCo_2O_4$ nanocomposites

Based on the refinement results in Table 2, it appears that two phases were formed, namely the Fe_3O_4 phase and the $NiCo_2O_4$ phase in the FN-15, FN-30, and FN-45 samples. This shows that the $Fe_3O_4/NiCo_2O_4$ nanocomposites which is supported by the X-ray diffraction patterns visually in Figure 2 formed characteristic peaks from each phase marked by ▲ which are the peaks of the Fe_3O_4 phase and • which are the peaks of the $NiCo_2O_4$ phase. A similar study was also conducted by Venugopal in 2020, which also produced characteristic peaks of both phases [29]. In addition, the results of this characterization also show that the more mass percent of $NiCo_2O_4$ added, the higher the peak of each material. With the addition of $NiCo_2O_4$ mass of 45%, the peak of $NiCo_2O_4$ particles has the highest peak, and all peaks of the composite material are increasingly visible. This can be indicated that the addition of 45% $NiCo_2O_4$ mass is the optimum mass. Meanwhile, with the

addition of 15% mass, there is an invisible peak of $NiCo_2O_4$. This is because the addition of the mass ratio between the two materials is not stable and tends to be seen with materials with a higher mass.

Table 2. Refinement results of the X-ray the diffraction patterns for the $Fe_3O_4/NiCo_2O_4$ nanocomposites

Parameters	FN-0	FN-15		FN-30		FN-45		FN-100
	Fe_3O_4	Fe_3O_4	$NiCo_2O_4$	Fe_3O_4	$NiCo_2O_4$	Fe_3O_4	$NiCo_2O_4$	$NiCo_2O_4$
Crystallite size (nm)	15.6	14.2	34.7	9	49.5	10.4	51.2	50.1
Lattice parameters *a = b = c* (Å)	8.394	8.369	8.111	8.357	8.084	8.354	8.094	8.201
Wt %	100	88.70	11.30	61.53	38.47	61.53	38.47	100
Rp	25.43	26.25		27.42		29.39		38.67
Rwp	33.97	35.11		37.58		38.91		39.18
GoF	1.23	1.40		1.60		1.70		1.89

SEM images of the samples are presented in Figure 3. Figure 3(a) and 3(b) represent the surface morphology of the FN-15 sample with a magnification of 500x and 20000x, respectively. Figures 3(c) and 3(d) are the surface morphology of the FN-30 sample with a magnification of 500x and 20000x, respectively. Meanwhile, the surface morphology of the FN-45 sample with a magnification of 500x and 20000x is presented in Figures 3(e) and 3(f), respectively. Based on the images, the surface morphology image also contains information related to the level of agglomeration of the $Fe_3O_4/NiCo_2O_4$ nanocomposites. The images also show that the Fe_3O_4 and $NiCo_2O_4$ have wide gaps between particles. So that increasing the material used for potential absorbance applications, the wider the surface area, the higher the absorbance. Based on research conducted by Tian et al., the morphology of $NiCo_2O_4$ can be modified according to various methods and treatments [22], resulting in various morphological forms and various advantages according to their morphological forms.

The characterization also obtained the weight percent of each constituent compound. With the addition of 15% of $NiCo_2O_4$ mass, the percentage of Fe content was 57.26 wt%, O content was 33.71 wt%, Ni content was 2.05%, and Co content was 3.41 wt%. Meanwhile, the addition of 30% $NiCo_2O_4$ mass, the Fe content was 3.6 wt%, the O content was 19.43 wt%, the Ni content was 25.69%, and the Co content was 51.28 wt%, and the addition of $NiCo_2O_4$ mass by 45%, as a percentage of Fe content of 2.99 wt%, O content of 47.25 wt%, Ni content of 16.45 wt%, and Co content of 33.31 wt%. With the addition of 45%, $NiCo_2O_4$ mass having a very high oxygen content, oxidation can occur during the synthesis process. Based on the data in Figures 3(g-i), it is found that the particle size of each sample FN-15 (g) is 3.8 µm; FN-30 is 2.8 µm; and FN-45 is 3.4 µm.

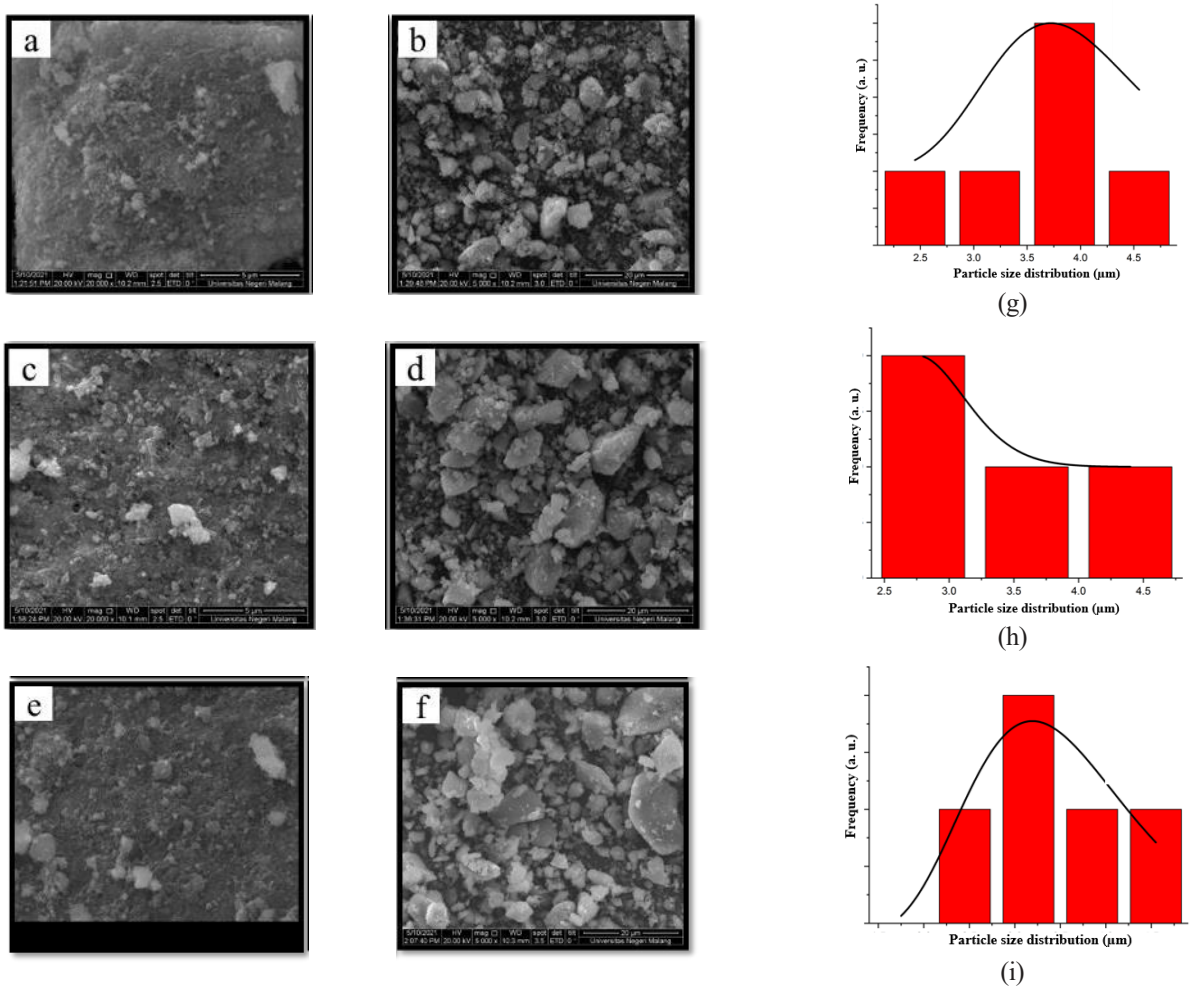


Fig. 3. SEM images of (a) FN-15 sample with 500x magnification; (b) FN-15 sample with a magnification of 20000x; (c) FN-30 sample with 500x magnification; (d) FN-30 sample with a magnification of 20000x; (e) FN-15 sample with 500x magnification; (f) FN-15 sample with a magnification of 20000x; (g) histogram of the particle size distribution of FN-15 sample; (h) histogram of the particle size distribution of FN-30 sample; (i) histogram of the particle size distribution of FN-45 sample.

The results of the characterization using FTIR are presented in Figure 4. Based on Figure 4, it can be seen that there are Ni-O and Co-O functional groups in the wavenumbers of 532 cm^{-1} and 647 cm^{-1} [30]. This shows that the $NiCo_2O_4$ material is indicated in the synthesis of nanocomposites, at that wavenumber a very sharp peak occurs. At the peak of 532 cm^{-1} induced by Co-N stretching, indicating the coordination of Co and N in Ni-Co, this study was carried out by Wang *et al.* in 2021 [31]. There is a Fe-O functional group in the wavenumber

of 536 cm^{-1} [32–34]. In addition, there are various functional groups identified at wavenumbers of 3515, 1725, 1305, 532, 647, and 536 cm^{-1}. The absorbance type appears with N-H bonds at the wavenumber of 1589 cm^{-1}. Therefore, the materials and composites in this study are suitable for use as absorbance applications. The data analysis results of the FTIR spectra are shown in Table 3.

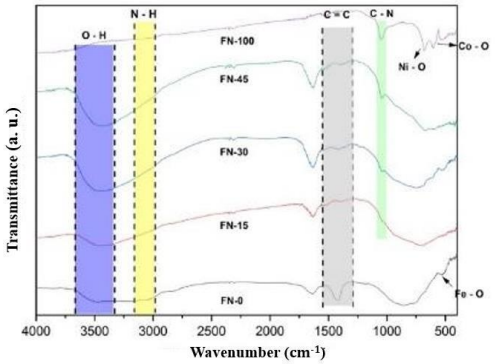


Fig. 4. FTIR spectra of the $Fe_3O_4/NiCo_2O_4$ nanocomposites

Table 3. The data analysis results of the FTIR spectra for $Fe_3O_4/NiCo_2O_4$ nanocomposites

Wavenumber (cm^{-1}) Model	Wavenumber (cm^{-1}) Experimental data	Bonding Characteristics	References
4000 – 3000	3515	O -H	[35–37]
3310 – 3500	3310	N-H	[4]
1575 – 1440	1725	C=C	[38]
1300 – 1000	1305	C-N	[36, 37]
532	532	Ni-O	[30]
647	647	Co-O	[30]
472 – 580	536	Fe-O	[32–34]

The purpose of the synthesis of $Fe_3O_4/NiCo_2O_4$ nanocomposites was to determine its potential application as photodegradation of methylene blue. This characterization process was carried out with several pre-characterization stages. The first step is to put the $Fe_3O_4/NiCo_2O_4$ nanocomposites into the MB solution without stirring. In the next stage, the product from the previous stage was irradiated with UV lamps with several variations of time-lapse. After these steps had been completed, the characterization using UV-Vis was ready to be carried out. Figure 5 is a photo of the MB solution containing the $Fe_3O_4/NiCo_2O_4$ nanocomposites which had been irradiated by UV lamp. In this study, a 10 watt UV lamp was used and the irradiation was carried out continuously from 60 minutes to 180 minutes. The mixture of MB solution with a concentration of 20 ppm which has been tested using UV-Vis Spectrophotometry has a wavenumbers of 613 and 663 nm, as shown in Figure 6.

The photodegradation process can be broadly divided into three stages, namely, diffusion, absorbance, and desorption. The diffusion process generally occurs at the surface before the irradiation occurs. The percentage degradation of $Fe_3O_4/NiCo_2O_4$ nanocomposite is presented in Figure 7. The straightline equation $y = 0.218x\text{-}0.001$ with the coefficient of determination (R^2) is 0.998. The value of the coefficient of determination meets the standard because 37as t close to the value 1, where this value indicates the feasibility of using graphs in testing [39]. So that in this study the UV-Vis characterization refers to the research related to the wavelength that is fired and also the standardization of the MB solution. In this study, the analysis of the wavelength of the MB standard solution has a maximum absorbance level at a wavenumber of 600-700 nm. This is possible because 37as t a complementary color at that wave number to the standard methylene blue solution [40], and the maximum absorbance level was obtained at wavelengths of 613 and 663 nm with an average absorbance value of 2.5.

The results of UV-Vis characterization showed that the average absorbance peak was in the range of 1-3. The diffusion ability is influenced by the surface area and also the structure of the nanocomposite. The larger the surface area, the higher the measured diffusion percentage. 37as tis the absorbance process in which electron transfer occurs between MB hydroxyl carbon and nanocomposite by continuously adding energy for 60 minutes. Then, the 37as tis the desorption process, namely the release of ions that have been bound to MB [7], with the highest percentage of degradation in the FN-45 sample reaching 11.99%, as shown in Figure 7. This proves that the more concentration of $NiCo_2O_4$ added, the higher the absorbance level is influenced by the length of UV irradiation for 180 minutes. The longer the time used for irradiation, the better and the higher the absorbance level. From the analysis of UV-Vis results, it is shown that the $Fe_3O_4/NiCo_2O_4$ nanocomposites was successfully used as a material for photodegradation applications.

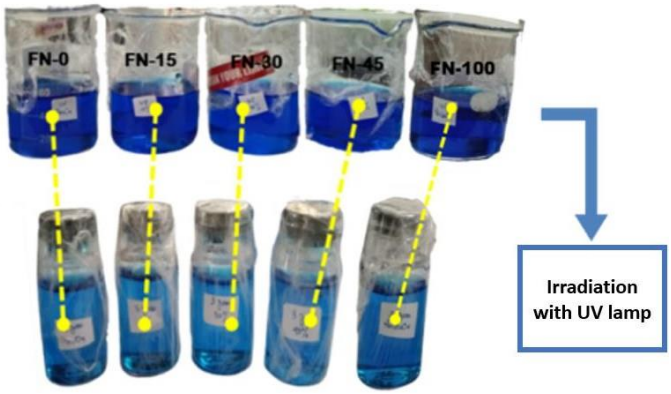


Fig. 5. MB solution containing the $Fe_3O_4/NiCo_2O_4$ nanocomposites after irradiation with UV lamp.

Table 5. Average absorbance of MB standard solution

MB Concentration (ppm)	Absorbance
0	0
1	0.22
2	0.418
3	0.666
4	0.892

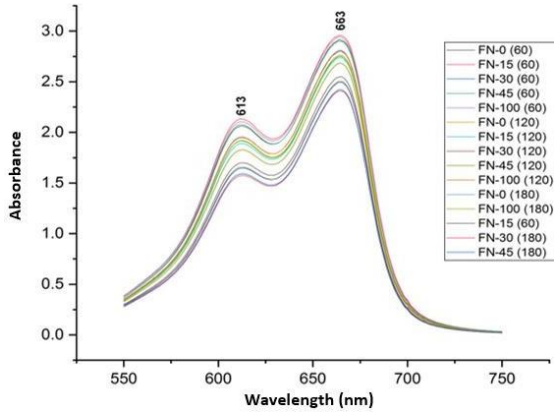


Fig. 6. Absorbance of the $Fe_3O_4/NiCo_2O_4$ nanocomposites

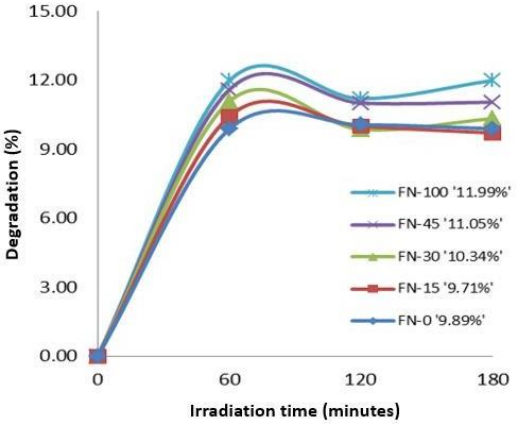


Fig. 7. Degradation of the $Fe_3O_4/NiCo_2O_4$ nanocomposites

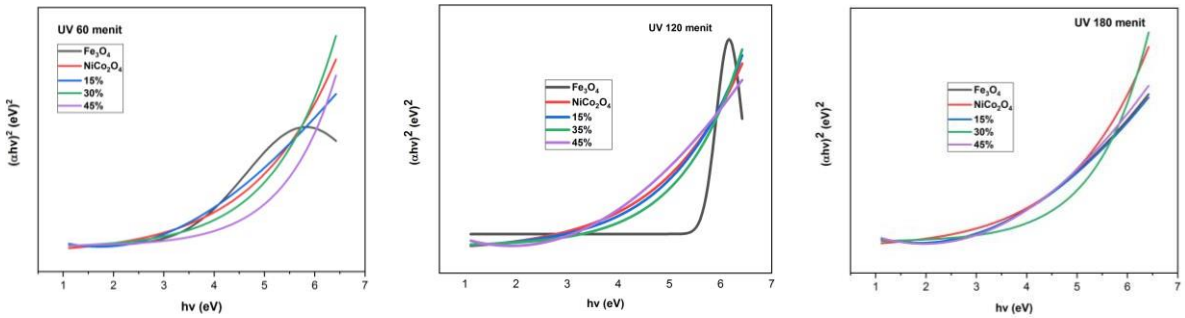


Fig. 8. The graphs of $(\alpha hv)^2$ vs hv of the $Fe_3O_4/NiCo_2O_4$ nanocomposites

The bandgap is the difference between the conduction energy and valence energy levels [41]. Figure 8 shows the bandgap curve obtained from the cutting wavelength of the absorbance spectrum of the composite material. The search for the value of the bandgap can be found using the Tauc curve. The equation is as follows:

$$(\alpha hv)^2 = A(hv - E_g) \quad (1)$$

where α is the absorption coefficient, A is the effective mass of electrons, h is the Planck's constant which is 6.63×10^{-34} Js, and v is the frequency. The UV-Vis data is then transformed to get the Tauc curve to determine the band gap value. Bandgap values can be obtained through the results of linear fitting between graphs $(\alpha hv)^2$ and hv as X and Y axis.

Table 6. Bandgap values of the $Fe_3O_4/NiCo_2O_4$ nanocomposites

Time	Sample Variation	Bandgap (eV)
60 minutes	Fe_3O_4	3.1
	$NiCo_2O_4$	3.4
	15%	2.8
	30%	3.7
	45%	1.1
120 minutes	Fe_3O_4	5.5
	$NiCo_2O_4$	3.8
	15%	3.7
	30%	3.7
	45%	2.9
180 minutes	Fe_3O_4	2.9
	$NiCo_2O_4$	3.4
	15%	3.1
	30%	4.0
	45%	3.4

4. Conclusions

$Fe_3O_4/NiCo_2O_4$ nanocomposites were successfully synthesized using the coprecipitation method. The X-ray diffraction pattern from the XRD instrument shows that there are two phases formed, namely the Fe_3O_4 phase and the $NiCo_2O_4$ phase. Based on the test results using SEM-EDX, an image of the surface morphology of the sample and the percentage of its constituent compounds is dominated by Fe, Ni, Co, and O compounds. While characterization using FTIR obtained vibrations due to Ni-O and Co-O bonds, each of which lies at the wavenumbers of 532 cm^{-1} and 647 cm^{-1}. In addition, there is also a vibration at the wavenumber of 536 cm^{-1} occupied by the Fe-O functional group as a constituent of Fe_3O_4 compounds. The photodegradation characterization resulted in the absorbance value of $Fe_3O_4/NiCo_2O_4$ nanocomposites

which were at wavenumbers of 613 nm and 663 nm. It can be said that the $Fe_3O_4/NiCo_2O_4$ nanocomposites can be used as a catalyst for water purification with a degradation percentage of 11.99%.

References

[1] I. Nurhaliza and R. N. Sunarti, "Analisa Residu Detergen pada Sampel Air Sungai di Provinsi Sumatera Selatan Secara MBAS menggunakan Spektrofotometri UV-Vis," vol. 3, no. 1, p. 10, 2020.
[2] T. B. Prayogo, "Analisis Kualitas Air Dan Strategi Pengendalian Pencemaran Air Sungai Metro di Kota Kepanjen Kabupaten Malang," p. 10.
[3] A. S. H. Wahyuni, "Sintesis karbon dots berbasis eceng gondok (Eichornia Crassipes) dengan doping seng oksida sebagai," p. 35, 2019.
[4] Erwanto, "Pengaruh Penambahan Ion Nitrat (NO^{3-}) terhadap Kinetika Fotodegradasi Zat Warna Metilen Biru Menggunakan Zeolit-TiO_2," vol. 5, pp. 59–67, 2020.
[5] A. Ramadhani and A. Linggawati, "Kapasitas adsorpsi metilen biru oleh lempung cengar teraktivasi asam sulfat," vol. 2, p. 7, 2015.
[6] A. Maddu, E. Palupi, and S. Pramudito, "Pengaruh konsentrasi awal dan penambahan H_2O_2 terhadap efektivitas degradasi fotokatalisis methylene blue pada film TiO_2," p. 8.
[7] M. Petit, L. Michez, J.-M. Raimundo, T. Malinowski, and P. Dumas, "An introduction to photocatalysis through methylene blue photodegradation," *Eur. J. Phys.*, vol. 37, no. 6, p. 065808, Nov. 2016, doi: 10.1088/0143-0807/37/6/065808.
[8] V. A. S. Augustia, I. D. Lestari, and M. D. Rani, "Degradasi Limbah Zat Warna Direk Dengan Metode Advanced Oxidation Processes (AOPs) Kombinasi H2O2/MnO2 dengan Parameter Uji BOD, COD dan pH," *Eksergi*, vol. 15, no. 1, p. 5, Jul. 2018, doi: 10.31315/e.v15i1.2249.
[9] F. Fina, H. Ménard, and J. T. S. Irvine, "The effect of Pt NPs crystallinity and distribution on the photocatalytic activity of Pt–g-C_3N_4," *Phys. Chem. Chem. Phys.*, vol. 17, no. 21, pp. 13929–13936, 2015, doi: 10.1039/C5CP00560D.
[10] F. Chen, H. Yang, W. Luo, P. Wang, and H. Yu, "Selective adsorption of thiocyanate anions on Ag-modified g-C_3N_4 for enhanced photocatalytic hydrogen evolution," *Chinese J. Catal.*, vol. 38, no. 12, pp. 1990–1998, Dec. 2017, doi: 10.1016/S1872-2067(17)62971-1.
[11] X. Xu, J. Luo, L. Li, D. Zhang, Y. Wang, and G. Li, "Unprecedented catalytic performance in amine syntheses *via* Pd/g-C_3N_4 catalyst-assisted transfer hydrogenation," *Green Chem.*, vol. 20, no. 9, pp. 2038–2046, 2018, doi: 10.1039/C8GC00144H.
[12] Y. Fu *et al.*, "High-performance NiO/g-C_3N_4 composites for visible-light-driven photocatalytic overall water splitting," *Inorg. Chem. Front.*, vol. 5, no. 7, pp. 1646–1652, 2018, doi: 10.1039/C8QI00292D.
[13] Y. Liu *et al.*, "Novel visible light-induced g-C3N_4–Sb_2S_3/$Sb_4O_5Cl_2$ composite photocatalysts for efficient degradation of methyl orange," *Catal. Commun.*, vol. 70, pp. 17–20, Oct. 2015, doi: 10.1016/j.catcom.2015.07.015.
[14] M. Wang, S. Cui, X. Yang, and W. Bi, "Synthesis of g-C_3N_4/Fe_3O_4 nanocomposites and application as a new sorbent for solid phase extraction of polycyclic aromatic hydrocarbons in water samples," *Talanta*, vol. 132, pp. 922–928, Jan. 2015, doi: 10.1016/j.talanta.2014.08.071.
[15] K. He, J. Xie, M. Li, and X. Li, "In situ one-pot fabrication of g-C_3N_4 nanosheets/NiS cocatalyst heterojunction with intimate interfaces for efficient visible light photocatalytic H 2 generation," *Appl. Surf. Sci.*, vol. 430, pp. 208–217, Feb. 2018, doi: 10.1016/j.apsusc.2017.08.191.
[16] J. Fu, C. Bie, B. Cheng, C. Jiang, and J. Yu, "Hollow CoS $_x$ Polyhedrons Act as High-Efficiency Cocatalyst for Enhancing the Photocatalytic Hydrogen Generation of g-C_3N_4," *ACS Sustain. Chem. Eng.*, vol. 6, no. 2, pp. 2767–2779, Feb. 2018, doi: 10.1021/acssuschemeng.7b04461.
[17] D. Zeng *et al.*, "Toward noble-metal-free visible-light-driven photocatalytic hydrogen evolution: Monodisperse sub–15 nm Ni_2P nanoparticles anchored on porous g-C_3N_4 nanosheets to engineer 0D-2D heterojunction interfaces," *Appl. Catal. B Environ.*, vol. 221, pp. 47–55, Feb. 2018, doi: 10.1016/j.apcatb.2017.08.041.
[18] R. Shen, J. Xie, H. Zhang, A. Zhang, X. Chen, and X. Li, "Enhanced Solar Fuel H $_2$ Generation over g-C_3N_4 Nanosheet Photocatalysts by the Synergetic Effect of Noble Metal-Free Co_2P Cocatalyst and the Environmental Phosphorylation Strategy," *ACS Sustain. Chem. Eng.*, vol. 6, no. 1, pp. 816–826, Jan. 2018, doi: 10.1021/acssuschemeng.7b03169.
[19] H. Yang, R. Cao, P. Sun, X. Deng, S. Zhang, and X. Xu, "Highly dispersed and noble metal-free MPX (M = Ni, Co, Fe) coupled with g-C_3N_4 nanosheets as 0D/2D photocatalysts for hydrogen evolution," *Appl. Surf. Sci.*, vol. 458, pp. 893–902, Nov. 2018, doi: 10.1016/j.apsusc.2018.07.149.
[20] S. X. Liu, X. Y. Chen, and X. Chen, "A TiO_2/AC composite photocatalyst with high activity and easy separation prepared by a hydrothermal method," *J. Hazard. Mater.*, vol. 143, no. 1–2, pp. 257–263, May 2007, doi: 10.1016/j.jhazmat.2006.09.026.
[21] M. M. Khan, S. F. Adil, and A. Al-Mayouf, "Metal oxides as photocatalysts," *J. Saudi Chem. Soc.*, vol. 19, no. 5, pp. 462–464, Sep. 2015, doi: 10.1016/j.jscs.2015.04.003.
[22] Y. Tian et al., "Synthesis of $NiCo_2O_4$ nanostructures with different morphologies for the removal of methyl orange," *Appl. Surf. Sci.*, p. 7, 2017.
[23] S. Bharathi, D. Nataraj, D. Mangalaraj, Y. Masuda, K. Senthil, and K. Yong, "Highly mesoporous α-Fe_2O_3 nanostructures: preparation, characterization and improved photocatalytic performance towards Rhodamine B (RhB)," *J. Phys. D. Appl. Phys.*, vol. 43, no. 1, p. 015501, Jan. 2010, doi: 10.1088/0022-3727/43/1/015501.
[24] R. Ermawati and E. Ratnawati, "Sintesis Nanopartikel Magnetit Dengan Metode Dekomposisi Termal," *J. Kim. dan Kemasan*, vol. 33, no. 1, p. 96, Apr. 2011, doi: 10.24817/jkk.v33i1.1834.
[25] Q. Liu, J. Ma, Y. Zhou, and T. Wang, "Synthesis of MgO-Modified mesoporous silica and its adsorption performance toward CO_2," *Wuhan Univ. J. Nat. Sci.*, vol. 19, no. 2, pp. 111–116, Apr. 2014, doi: 10.1007/s11859-014-0986-4.
[26] Z.-Q. Liu *et al.*, "Fabrication of hierarchical flower-like super-structures consisting of porous $NiCo_2O_4$ nanosheets and their electrochemical and magnetic properties," *RSC Adv.*, vol. 3, no. 13, p. 4372, 2013, doi: 10.1039/c3ra23084h.
[27] W. Chang, W. Xue, E. Liu, J. Fan, and B. Zhao, "Highly efficient H2 production over $NiCo_2O_4$ decorated g-C_3N_4 by photocatalytic water reduction," *Chem. Eng. J.*, vol. 362, pp. 392–401, Apr. 2019, doi: 10.1016/j.cej.2019.01.021.
[28] C. Yuan, J. Li, L. Hou, X. Zhang, L. Shen, and X. W. D. Lou, "Ultrathin Mesoporous $NiCo_2O_4$ Nanosheets Supported on Ni Foam as Advanced Electrodes for Supercapacitors," *Adv. Funct. Mater.*, vol. 22, no. 21, pp. 4592–4597, Nov. 2012, doi: 10.1002/adfm.201200994.
[29] R. Venugopal, K. Dhanyaprabha, H. Thomas, and R. Sini, "Optical characterisation of cadmium doped Fe_3O_4 ferrofluids by co-precipitation method," *Mater. Today Proc.*, vol. 25, pp. A1–A5, 2020, doi: 10.1016/j.matpr.2020.03.142.
[30] S. Chen and S.-Z. Qiao, "Hierarchically Porous Nitrogen-Doped Graphene–$NiCo_2O_4$ Hybrid Paper as an Advanced Electrocatalytic Water-Splitting Material," *ACS Nano*, vol. 7, no. 11, pp. 10190–10196, Nov. 2013, doi: 10.1021/nn404444r.
[31] M. Wang *et al.*, "Activating Peroxydisulfate with Co3O4/NiCo2O4 Double-Shelled Nanocages to Selectively Degrade Bisphenol AA Nonradical Oxidation Process," *Appl. Catal. B*, no. Query date: 2020–11–05 00:21:25, 2020.
[32] M. Khatami *et al.*, "Leishmanicidal Activity of Biogenic Fe_3O_4 Nanoparticles," *Sci. Pharm.*, vol. 85, no. 4, p. 36, Nov. 2017, doi: 10.3390/scipharm85040036.
[33] M. Arakha *et al.*, "Antimicrobial activity of iron oxide nanoparticle upon modulation of nanoparticle-bacteria interface," *Sci. Rep.*, vol. 5, no. 1, p. 14813, Dec. 2015, doi: 10.1038/srep14813.
[34] H.-M. Xiong, D. G. Shchukin, H. Möhwald, Y. Xu, and Y.-Y. Xia, "Sonochemical Synthesis of Highly Luminescent Zinc Oxide Nanoparticles Doped with Magnesium(II)," *Angew. Chemie Int. Ed.*, vol. 48, no. 15, pp. 2727–2731, Mar. 2009, doi: 10.1002/anie.200805590.
[35] L. Dian *et al.*, "Enhancing oral bioavailability of quercetin using novel soluplus polymeric micelles," *Nanoscale Res. Lett.*, vol. 9, no. 1, p. 684, 2014, doi: 10.1186/1556-276X-9-684.
[36] Q. A. Lathifah, "Uji efektifitas ekstrak kasar senyawa antibakteri pada buah belimbing wuluh (Averrhoa bilimbi L.) dengan variasi pelarut," undergraduate, Universitas Islam Negeri Maulana Malik Ibrahim, 2008.
[37] I. M. Sukadana, "Senyawa antibakteri golongan flavonoid dari buah belimbing manis (Averrhoa carambola Linn. L)," *J. Kim.*, vol. 3, no. 2, 2009.
[38] M. Diantoro, T. Suprayogi, A. Taufiq, A. Fuad, and N. Mufti, "The Effect of PANI Fraction on Photo Anode Based on TiO_2-PANI /ITO DSSC with β-carotene as Dye Sensitizer on its Structure, Absorbance, and Efficiency," *Mater. Today Proc.*, vol. 17, pp. 1197–1209, 2019, doi: 10.1016/j.matpr.2019.05.345.
[39] T. Huda and T. K. Yulitaningtyas, "Kajian Adsorpsi Methylene Blue Menggunakan Selulosa dari Alang-Alang," vol. 01, no. 01, p. 11, 2018.
[40] A. Nurzihan, R. U. N. Hrp, S. H. Siregar, and H. Nasution, "Adsorpsi zat warna methylene blue menggunakan bentonit termodifikasi ethylene diamine tetra aceticacid (EDTA)," vol. 1, p. 13, 2019.
[41] A. Q. A'Yun, "Aplikasi karbon dots (cds) organik sebagai katalisator dalam proses fotodegradasi metilen biru dengan sinar ultraviolet," p. 67, 2018.